CHAPTER II

LITERATURE REVIEW

2.1 Introduction to the Mössbauer Effect

An atomic nucleus can undergo transitions from its ground state to its excited states and vice versa. These transitions are often accompanied by an absorption or emission of a quantum of electromagnetic radiation. Such a quantum or photon emitted by one nucleus may be absorbed by another nucleus of the same kind (isotope) exciting the latter to a higher level. This process is called "resonant absorption" and only occurs when the emission and the absorption lines sufficiently overlap (Fig. 2.1). The two lines do not coincide exactly owning to a recoil momentum which is imparted to the emitting nucleus, consuming a part of the transition energy, leaving a somewhat smaller energy for the photon than the energy difference between the nuclear levels. If the emission and absorption lines are narrow, the recoil energy may be sufficient to prevent any overlap of the two lines and resonant absorption does not occur.

In order to see the situation clearly, let us consider a free nuclear system, of mass M, with two levels, ground state A and excited state B, separated by an energy E_T. If the system decays from B to A by emission of a photon of energy E_γ, momentum conservation demands that the momentum $\vec{p}$ of the photon and the momentum $\vec{P}$ of the recoiling system be equal and opposite. Hence the recoiling system receives an

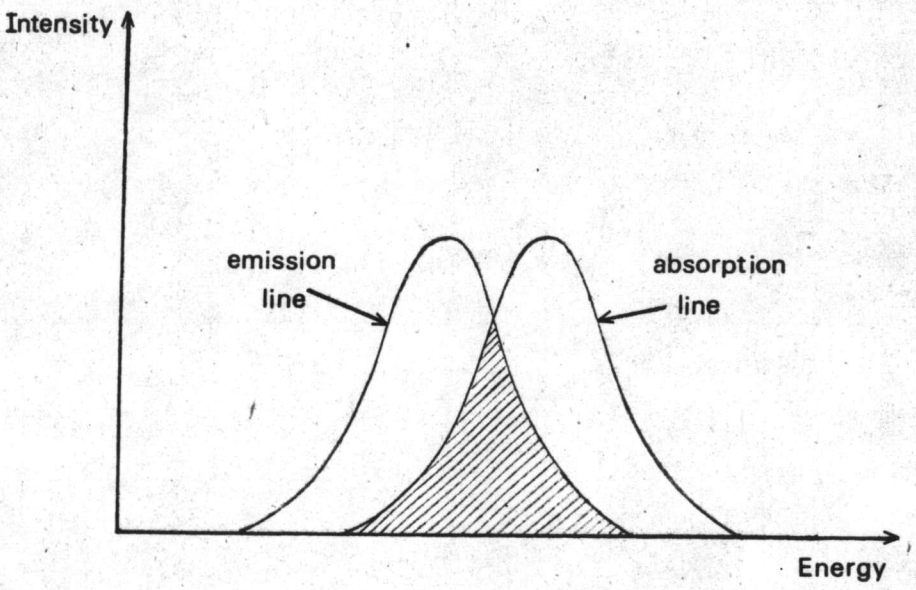

Fig. 2.1. Line profiles for emission and absorption of a γ - quantum by a nucleus. The lines are shifted owing to recoil. Resonant absorption of emitted quanta occurs in proportion to the overlap between the two lines (shaded area).

energy E_R , given by

$$E_R = \frac{P^2}{2M} = \frac{p^2}{2M} = \frac{E_\gamma^2}{2Mc^2} \qquad (2.1.1).$$

In this derivation, it is assumed that the recoiling system can be treated nonrelativistically. Energy conservation connects E_T , E_γ , and E_R by the requirement that

$$E_T = E_\gamma + E_R \qquad (2.1.2).$$

Since E_R is very small compared to E_γ , E_γ can be replaced by the transition energy E_T in eq. (2.1.1) :

$$E_R \simeq \frac{E_T^2}{2Mc^2} \qquad (2.1.3).$$

For a quick evaluation, eq. (2.1.3) can be rewritten into the numerical form (May, 1971)

$$E_R \text{ (in eV)} = \frac{5.37 \times 10^{-4} \; E_T^2 \text{ (in KeV)}}{A} \qquad (2.1.4),$$

where A is the mass number of the decaying nucleus.

Since the excited state B has the mean life τ , and according to the Heisenberg uncertainty relation, the energy in the state cannot be measured exactly. It can be measured only to within an uncertainty given by

$$\tau \cdot \Gamma = \hbar \qquad (2.1.5),$$

where $2\pi\hbar$ is Planck's constant. The uncertainty is given by the numerical relation (May, 1971)

$$\Gamma \text{ (in eV)} = 6.58 \times 10^{-16}/\tau \text{ (sec)} \qquad (2.1.6).$$

Thus the decaying state B cannot be characterized by one well defined energy E_T only, but that the energy E of the state is distributed about the center energy E_T having the full width of the energy distribution of Breit-Wigner shape at half-height Γ as shown in Fig. 2.2 a. The energy of the stable ground state, according to eq. (2.1.5), is sharp since τ is infinite. Photons emitted in the transition from B to A thus show a distribution in energy E_γ, centered around $E_T - E_R$, and displaying a "natural line shape" of width Γ (see Fig. 2.2 b).

When a photon of energy E_γ and momentum $\vec{p}$ strikes a target of mass M, initially at rest, the entire momentum $\vec{p}$ is tranformed to the target. It thus recoils and the energy of recoil E_R is given by eq. (2.1.3). This energy must be supplied by the gamma ray. Then only an energy $E_T - E_R$ is avialable for the excitation of internal degrees of freedom. In order to excite a level of energy E_T, the incoming gamma photon must have an energy $E_T + E_R$, as shown in Fig. 2.2 c. Resonant absorption can occur only if some of the incoming photons possess enough energy to reach the state B and at the same time provide the energy E_R for the recoiling system. Thus only the overlapping part of the spectra 2.2b and 2.2c is responsible for resonant absorption (see Fig. 2.2 d). The condition for overlap is

$$2R \lesssim \Gamma \qquad (2.1.7).$$

For a typical case (^{57}Fe), the transition energy is 14.4 KeV with a mean life τ of 10^{-7} sec. Equations (2.1.4) and (2.1.6) give

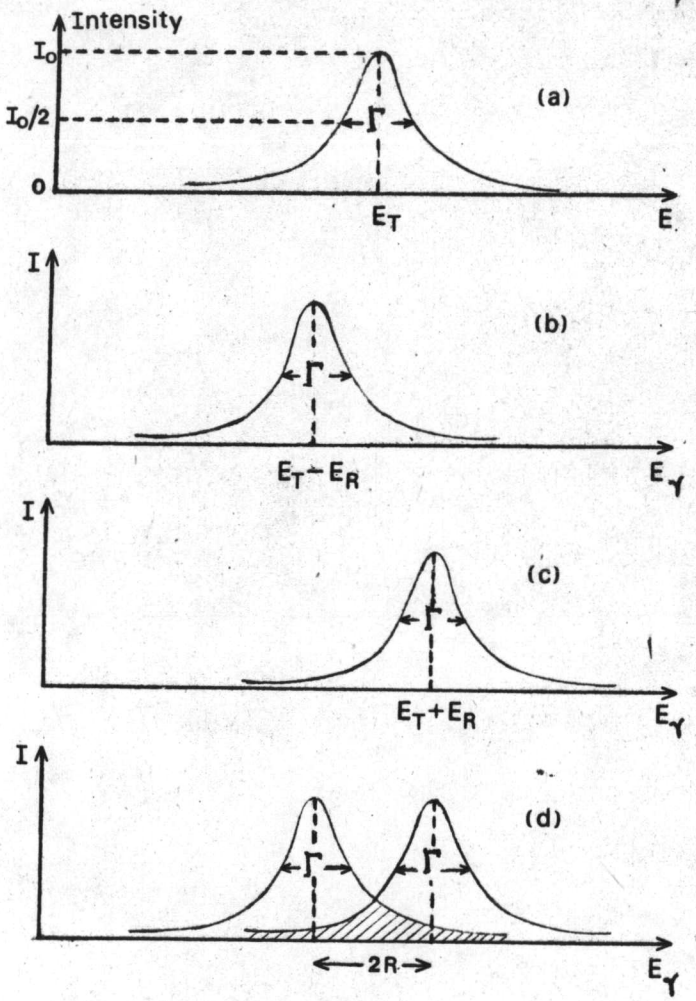

Fig. 2.2. Energy distribution of Breit – Wigner shape involved in resonant absorption. (a) Energy distribution of excited state B. (b) Energy distribution of photons emitted in a transition B → A. (c) Energy spectrum required to excite state B in target. (d) Overlap of (b) and (c).

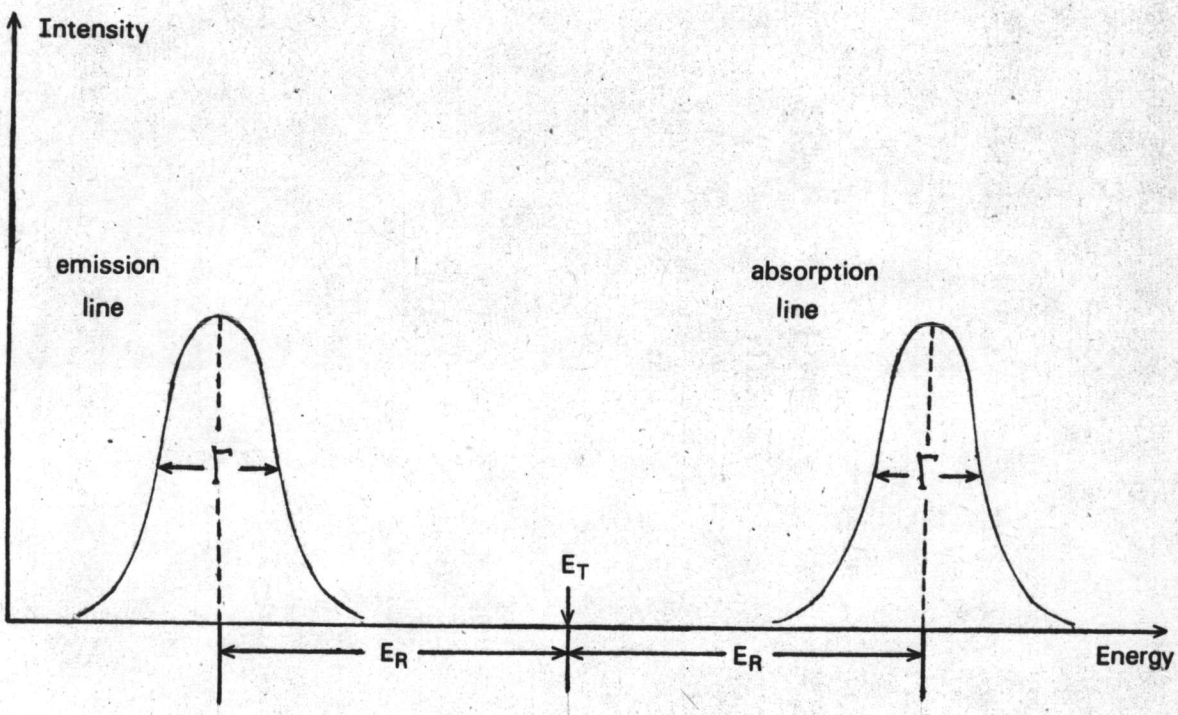

Fig.2.3. Resonant absorption is not possible if the recoil energy loss exceeds the linewidth.

$E_R = 1.95 \times 10^{-3}$ eV , and $\Gamma = 6.58 \times 10^{-9}$ eV respectively. The recoil energy is indeed small compared to the transition energy. It is, however, very large compared to the natural linewidth. As a result, the gamma-ray emission line does not overlap the absorption line, and nuclear resonance absorption cannot be observable, as shown in Fig. 2.3.

In the case of atomic radiation, i.e., light resulting from electronic transitions, the energy of the emitted quantum is 10^4 times smaller while the inherent line-widths are the same as in the nuclear case. The recoil energy (order of 10^{-11} eV) is thus smaller than the linewidth, so that resonant absorption is readily observable.

When the emitting atom is confined in a crystal lattice, the recoil momentum connot be absorbed solely by the atom, since the atom is bound to the crystal. The total energy of the γ-transition E_T must be conserved and can only be shared between

1) the energy of the γ - photon , E_γ ;

2) the lattice vibrations ;

3) the translational kinetic energy of the individual atom;

4) the translational kinetic energy of the solid as a whole.

The third of these possibilities is eliminated by the high chemical binding energy (order of 1 - 10 eV) , which is considerably greater than the free recoil energy E_R . For the second possibility to occur, the atom must be able to excite one or more of the vibrational modes of the lattice. When this occurs, the atom is said to have emitted a phonon. There exists also a finite probability that no phonon is emitted. Since the vibrational energy levels of the crystal lattice are quantised : only discrete energy

increments are allowed and unless the recoil energy corresponds closely to one of the allowed increments it cannot be transferred to the lattice. When the recoil does not produce a momentum change corresponding to the energy increment, the recoil momentum is imparted directly to the crystal as a whole. This is the least likely. Equation (2.1.3) becomes

$$E_R = \frac{E_T^2}{2m_c c^2} \qquad (2.1.10),$$

where m_c is the crystal mass. Even in a fine powder the crystalline system contains at least 10^{15} atoms (Greenwood and Gibb, 1971). This decreases E_R by a factor of 10^{15}.

For a typical ^{57}Fe case ($\Gamma = 6.58 \times 10^{-9}$ eV), eq. (2.1.10) becomes

$$E_R = 1.95 \times 10^{-3}/10^{15} = 1.95 \times 10^{-18} \text{ eV} \qquad (2.1.11).$$

Combining eqs. (2.1.2) and (2.1.11) gives approximately

$$E_\gamma = E_T \left(1 - \frac{E_T}{2m_c c^2}\right) = E_T \left(1 - 10^{-22}\right) \qquad (2.1.12).$$

This correction for the recoil is negligible and the emission is said to be "recoilless". By the same reasoning one can see that sometimes the absorption of the photon can also occur without emission of phonons. The two lines would have the very narrow natural linewidth Γ. The condition for overlap (eq. (2.1.7)] is fulfilled and thus the resonant absorption can be observed.

The effect of zero-phonon emission and resonant absorption of γ - quanta, the "Mössbauer effect", was first recognized by Mössbauer (1958) when investigating the nuclear resonant scattering of the 129 - KeV gamma ray from ^{191}Ir at low temperatures.

The possibility of zero-phonon emission is commonly expressed as the Mössbauer fraction f which indicates the number of zero-phonon emissions to the total number of γ - emissions. This fraction depends on the energy of the photon and the temperature as can be seen as follows. We again consider an atom confined in a crystal lattice. It performs a thermal vibration about its equilibrium position q with displacement Δq. We can therefore only be certain of finding the atom to within an interval $2\Delta q$. The Heisenberg uncertainty relation, then, leads to an uncertainty Δp in the linear momentum p given by

$$2\Delta q \Delta p \simeq \hbar \qquad (2.1.13).$$

We now let the atom emit a photon with momentum P_γ given by

$$P_\gamma = \frac{E_\gamma}{c} \qquad (2.1.14).$$

According to the previous discussion, the recoil momentum is imparted to the crystal either directly or via excitation of phonons. If P_γ is of the order of magnitude of Δp, it is impossible to tell whether the recoil momentum has been imparted to the atom or not. It is thus impossible to distinguish between the vibrational state of the atom before and after the emission. It must be concluded that the momentum is imparted to the crystal as a whole, without excitation of phonons. Thus if

$$P_\gamma \approx \hbar/2\Delta q \qquad (2.1.15),$$

there is a good chance for zero-phonon emission. With $2\Delta q \approx 10^{-11}$ m and $\hbar \approx 10^{-34}$ Js , we obtain $P_\gamma \approx 10^{-23}$ Js m^{-1} which is the momentum associated with a photon of 20 KeV by eq. (2.1.14).

From eq. (2.1.15) , we can see that since the thermal displacement Δq increases with increasing temperature, the Mössbauer fraction will decrease as the temperature increase. We also see that increase of the photon energy lowers the value of f . For various nuclei embedded in a crystal of their own element, the Mössbauer fraction at 0^oK is given as a function of the energy (see Fig. 2.4). The temperature dependence of f for ^{57}Fe is shown in Fig. 2.5.

The actual expression for the Mössbauer fraction f is

$$f = \exp\left[-\frac{1}{3} P_\gamma^2 \langle(\Delta q)^2\rangle\right] \qquad (2.1.16)$$

(Kittel,1963). Here $\langle(\Delta q)^2\rangle$ is the mean square of the displacement Δq of the atom from its equilibrium position. For a Debye solid this displacement is given by (Wohlfarth, 1967)

$$\langle(\Delta q)^2\rangle = \frac{9}{4}\frac{1}{MK\theta}\left\{1 + 4\left(\frac{T}{\theta}\right)^2 \int_0^{\theta/T} \frac{x\,dx}{e^x - 1}\right\} \qquad (2.1.17),$$

where M is the mass of the emitting or absorbing nucleus, K is Boltzmann constant, θ is the Debye temperature and T is the absolute temperature. Combining with eq. (2.1.16), we obtain

$$f = \exp\left[-\frac{3}{2}\frac{E_\gamma^2}{2Mc^2}\frac{1}{K\theta}\left\{1 + 4\left(\frac{T}{\theta}\right)^2 \int_0^{\theta/T} \frac{x\,dx}{e^x - 1}\right\}\right],$$

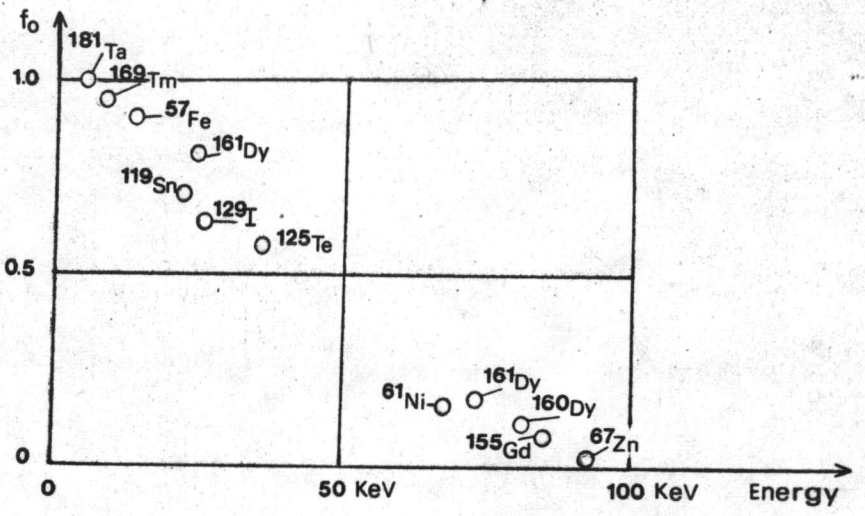

Fig.2.4. Mössbauer fraction at $0^{\circ}K$ as a function of the energy of the γ-quantum for various nuclei embedded in a crystal of their own element (Wohlfarth, 1967).

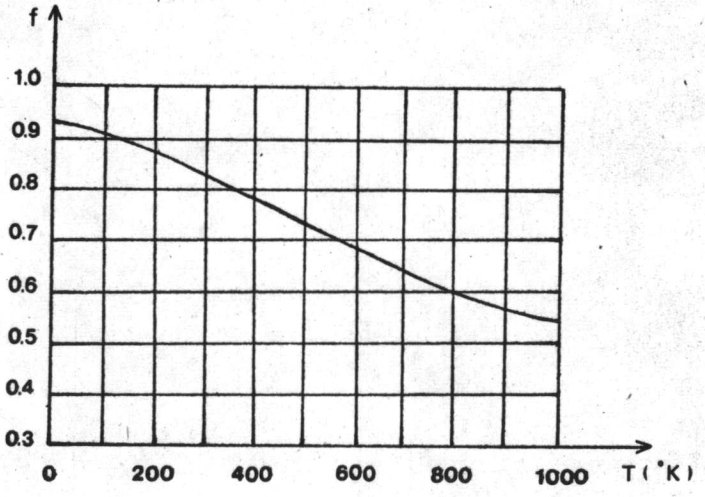

Fig. 2.5. Mössbauer fraction of ^{57}Fe embedded in stainless steel as a function of temperature. (Wohlfarth, 1967).

$$f = \exp\left[-\frac{3}{2}\frac{E_R}{K\theta}\left\{1 + 4\left(\frac{T}{\theta}\right)^2 \int_0^{\theta/T} \frac{x\,dx}{e^x - 1}\right\}\right] \qquad (2.1.18),$$

where E_R is the free atom recoil energy as described in eq. (2.1.1). The term 1 between the curly brackets is due to the zero-point vibrations that still have to be present at $0^\circ K$ owning to the uncertainty relation.

For high temperatures, $T \gtrsim \frac{\theta}{2}$, we can ignore the first term and expand the second to get

$$f = \exp\left[-\frac{6E_R T}{K\theta^2}\right] \qquad (2.1.19)$$

(May, 1971). According to eq. (2.1.19), f will decrease exponentially as T increases.

For low temperatures, $T \ll \theta$, we can extend the upper limit of the integral to infinity (Wertheim, 1964) and obtain

$$\int_0^\infty \frac{x\,dx}{e^x - 1} = \frac{\pi^2}{6} .$$

This gives

$$f = \exp\left[-\frac{3}{2}\frac{E_R}{K\theta}\left\{1 + \frac{2\pi^2 T^2}{3\theta^2}\right\}\right] \qquad (2.1.20).$$

In the limit of zero temperature this factor depends only on the ratio of the free atom recoil energy to the Debye temperature,

$$f = \exp\left[-\frac{3E_R}{2K\theta}\right] \qquad (2.1.21).$$

A simple calculation using eq. (2.1.4), for a nucleus of mass 100 in a lattice with a Debye temperature of $400^{\circ}K$, gives

$$f = \exp\left[-\left(\frac{E_T \text{ (in KeV)}}{65}\right)^2\right] \qquad (2.1.22).$$

This shows why the Mössbauer effect is limited to low energy gamma rays. Because of the square in the exponent, the Mössbauer fraction drops off rapidly when E_T exceeds 65 KeV. To date the Mössbauer effect has not been observed for gamma-ray energies greater than 155 KeV.

For a given temperature the value of Δq will be smaller when the Debye temperature of the solid is higher. This property may be used to increase the Mössbauer fraction, i.e., by embedding the emitting atoms in a solid with strong interatomic forces thus having a high Debye temperatures. Such solids usually show a great mechanical hardness.

So far, we have described the mechanism by which a γ-ray photon can be emitted without recoil and the same arguments apply to resonant absorption. To see whether this property has any real utility we must see if a stable isotope exists which combines suitable lifetime and energy in its first excited state. The most advantageous combination is found in ^{57}Fe which has been used in more experiments than all other isotopes used to date. Its properties are summaried in Table 2.1.

Properties	Ground state	First excited state
Energy (KeV)	0	14.41
Spin and parity	$\frac{1}{2}^-$	$\frac{3}{2}^-$
Magnetic moment (nm)	0.0903	-0.153
Quadrupole moment (barns)	0	0.29
Mean life (sec)	Stable	1.4×10^{-7}

Table 2.1. Properties of ^{57}Fe (internal conversion coefficient = 9.7 ± 0.2 , natural abundance = 2.19 %).

Next consideration must be given to the cross section, σ_o , for absorption of the gamma ray by the resonant isotope, which is given by (May, 1971)

$$\sigma_o = 2\pi\lambda\!\!\!^{-2} \frac{2I_B + 1}{2I_A + 1} \frac{1}{1 + \alpha} \qquad (2.1.23),$$

where I_A and I_B are the nuclear spins of the ground and the excited state, respectively, α is the internal conversion coefficient, and $2\pi\lambda\!\!\!^{-}$ is the wave length of the gamma ray. Using the relation between $\lambda\!\!\!^{-}$ and E_T in eq. (2.1.23), we obtain the expression

$$\sigma_o\ (cm^2) = \frac{2.45 \times 10^{-15}}{E_T^2\ (KeV)} \quad \frac{2I_B + 1}{2I_A + 1} \quad \frac{1}{1 + \alpha} \qquad (2.1.24).$$

The energy dependence of the absorption cross section (due to line shape of the absorption line) can be expressed as

$$\sigma(E) = \sigma_o \frac{(\Gamma_a/2)^2}{(E-E_T)^2 + (\Gamma_a/2)^2} \qquad (2.1.25),$$

where E_T is the transition energy and Γ_a is the full width of the resonance at half maximum absorption. In ^{57}Fe, from eq. (2.1.24), the cross section is 2.2×10^{-18} cm^2, which is about 200 times greater than that for the next most important process, photoelectric absorption. As a result, the resonant absorption process can dominate even when the resonant isotope is a minor constituent of the absorbing solid.

In conclusion, the relevant orders of magnitude of the energy terms are given in Table 2.2.

Mössbauer γ-ray energies (E_γ)	$10^4 - 10^5$ eV
Chemical binding	1 - 10 eV
Free atom recoil energy (E_R)	$10^{-4} - 10^{-1}$ eV
Lattice vibration phonon energies	$10^{-3} - 10^{-1}$ eV
Heisenberg natural linewidths (Γ)	$10^{-9} - 10^{-6}$ eV

Table 2.2. Some typical energies in Mössbauer effect (Greenwood and Gibb, 1971).

The natural line widths of Mössbauer γ - rays permit a high intrinsic resolution of 10^{-10} to 10^{-14} of the γ - ray energies. However, in the presence of free atom recoil and thermal broadening effects, the resolution drops to 10^{-6} to 10^{-9}.

It is important to emphasize that γ - ray energies cannot be measured with this accuracy on an absolute scale, indeed these energies are seldom known to better than 1 part in 10^4. In order to benefit from the preciseness of the natural linewidth, it is customary to have as a reference, an absorber in which the absorbing nuclei have the same chemical environment as the emitting nuclei in the source. By comparing the Mössbauer absorptions by the nuclei in the reference with the absorption by the same nuclei in an unknown, the shift in the nuclear levels caused by the change in environment surrounding the nuclei can be measured. The principle by means of which this measurement is based is the "Doppler effect".

A basic setup for a Mössbauer experiment and a typical result are sketched in Fig. 2.6. In the experiment to be described, the source and absorber are made from identical materials so that the energy levels of the radioactive nuclei and absorbing nuclei are the same. The source is moved with a velocity V with respect to the absorber. The gamma rays then undergo a Doppler shift ΔE,

$$\Delta E = \pm \frac{V}{C} E_T \qquad (2.1.26).$$

Fig. 2.6 displays only the simplest case, single line source and single line absorber, both showing the same natural linewidth. At large velocities,

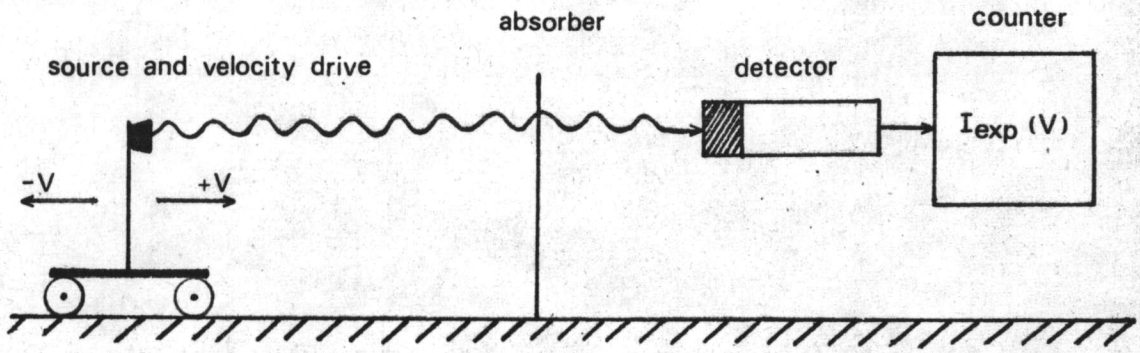

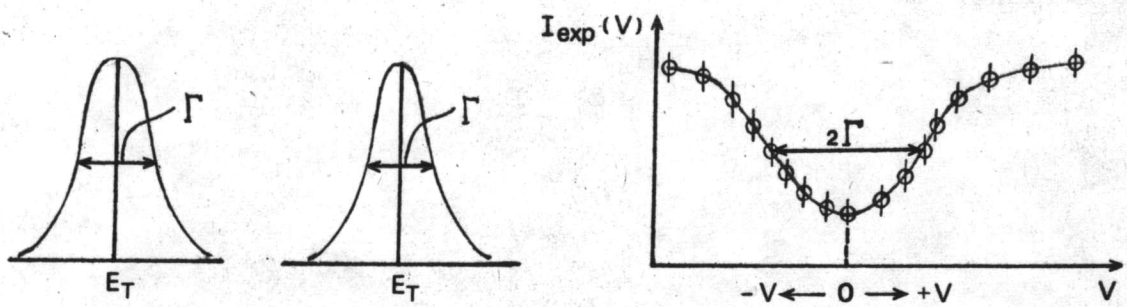

emission line

absorption line

spectrum observed as a function of the relative velocity V (thin source and thin absorber)

Fig. 2.6. Basic setup, emission and absorption lines, and velocity spectrum in a Mössbauer transmission experiment.

no resonant absorption occurs. The velocities at which resonant absorption becomes vanishingly small depend on the linewidths and the center of the transmitted line is at zero velocity if the centers of the emission and absorption lines are the same. In this case the transmitted line has a Breit-Wigner shape, but has an observed width of 2Γ. This broadening results from the overlap of the emission and absorption lines.

2.2 The Use of the Mössbauer Effect in the Study of the Magnetic Hyperfine Structure

This application of the Mössbauer effect to the study of the hyperfine structure depends on the narrowness of the linewidth of the gamma-emission and the shift in nuclear levels of the absorbing nuclei when it finds itself in a different environment from that of the emitting nuclei. The salient point is that the linewidths encountered are small compared to the characteristic energy of interaction between the nuclei with their surrounding electrons : those which arise from the coupling of the nuclear magnetic dipole moment with the magnetic electrons of the atom. A velocity spectrometer of the type discussed in Chapter III can be used to observe directly the magnetic hyperfine splitting of the nuclear energy levels.

To obtain a Mössbauer spectrum of a magnetic hyperfine splitting, we proceed as follows.

1) The radioactive material which will constitute the source is incorparated into a host where its nuclear levels remain unsplit.

Any cubic, diamagnetic metal will be a good choice provided the radioisotope enters the lattice substitutionally.

2) This source is then mounted on the "velocity transducer" which provides the motion for the Doppler shift.

3) A stationary absorber is now placed between the source and the detector.

Since the nuclear levels in the absorber are split by magnetic hyperfine interaction, there will be a number of different energies at which resonant absorption takes place. The counting rate at the detector will drop whenever the Doppler velocity applied to the source brings the energy of emitted γ - ray into coincidence with an absorption energy in the absorber.

The magnetic splitting arises from the interaction of the nuclear magnetic dipole moment $\vec{\mu}$ with a magnetic field, $\vec{H}$, due to the atom's own electrons. The Hamiltonian of the interaction is

$$\mathcal{H}_m = -\vec{\mu} \cdot \vec{H} = -g\,\mu_n\,\vec{I} \cdot \vec{H} \qquad (2.2.1),$$

and the energy levels which are obtained are

$$E_m = -g\mu_n H m_I = -\frac{\mu H m_I}{I}, \quad m_I = I, \ldots, -I \qquad (2.2.2),$$

where g is the nuclear g - factor, μ_n the nuclear magneton, $\vec{I}$ the nuclear spin, and m_I the magnetic quantum number. According to eq. (2.2.2) there are $2I + 1$ equally spaced levels; the splitting between adjacent levels is $g\mu_n H$ and the splitting between the lowest and the highest level is $2g\mu_n HI$.

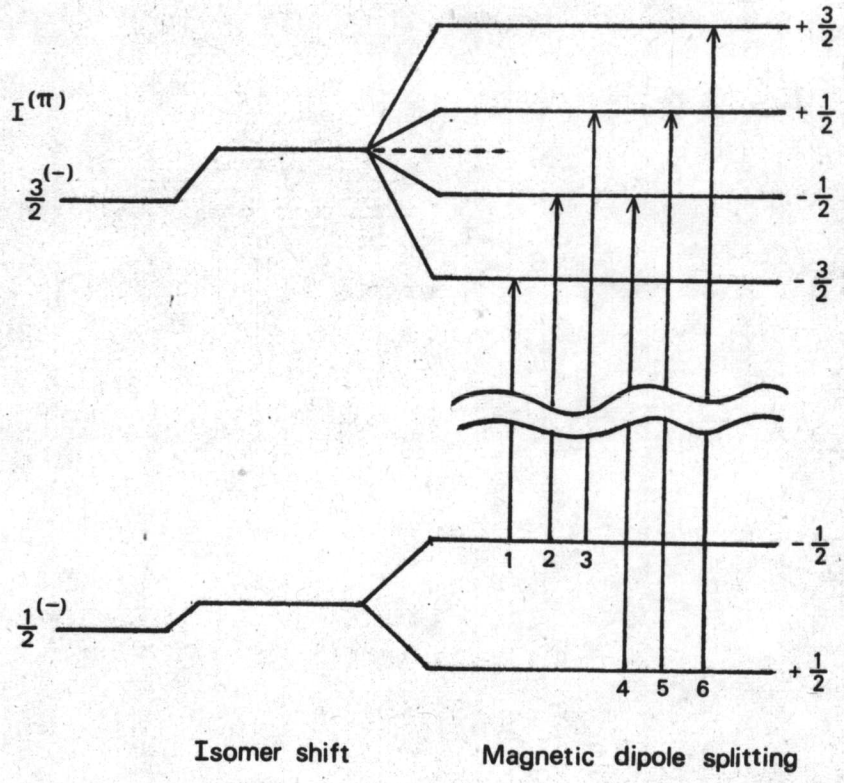

Fig. 2.7. Magnetic hyperfine splitting of the ground state and first excited state of ^{57}Fe. Note that the sign of nuclear magnetic moment of the ground state and excited states differ. The sixed allowed $\Delta m = 0, \pm 1$ transitions are indicated.

This interaction splits the degenerate I levels. For ^{57}Fe nucleus $I_{excited} = \frac{3}{2}$ and $I_{ground} = \frac{1}{2}$, the first level is split into four sub-levels, the second into two (Fig. 2.7). The gamma transition in ^{57}Fe from the excited to the ground state is of the magnetic dipole type and $\Delta m = \pm 1, 0$. Due to this condition only six transitions are possible. The relative intensities of the transition (for absorption) are given by $\left[(I_g m_g LM/I_e m_e)\right]^2 F_L^M(\theta)$ where $(I_g m_g LM/I_e m_e)$ is the Clebsch-Gordon coefficient describing the vector coupling of I_e and I_g through the radiation field LM ; θ is the angle between the direction of the magnetic field (axis of quantization) and the direction of observation and the radiation pattern $F_L^M(\theta)$ is given by $F_L^0(\theta) \propto \sin^2\theta$ and $F_L^{\pm 1}(\theta) \propto (1 + \cos^2\theta)$ for a magnetic dipole transition. For an unmagnetized absorber and with a single line source the relative intensities have to be averaged over θ and the ratio of the transition is 3 : 2 : 1 : 1 : 2 : 3. When the absorber is magnetized perpendicular to the γ - ray direction the intensity ratio is 3 : 4 : 1 : 1 : 4 : 3.

2.3 Magnetic Hyperfine Field in $CoFe_2O_4$ Spinel Ferrite

Before the theory is presented, several properties of the spinel ferrites will be given. They have the usual chemical formular such as $MO.Fe_2O_3$, where Fe yields a trivalent ion Fe^{3+} and M is a divalent ion, often Zn, Cd, Fe, Ni, Cu, Co, or Mg. Ferrites have the spinel crystal structure in which there are two types of sites of magnetic ions : one is tetrahedrally surrounded by four oxygen ions, and is called a tetrahedral site, or A site, whereas the other is surrounded octahedrally by six oxygen ions, and is called an octahedral, or B site. A unit cell of the spinel lattice has eight A sites and sixteen B sites. The eight A sites form the A sublattice while the sixteen B ones form the B sublattice. Since the following A sites are shared by four unit cells each,

$(\frac{1}{2}, 0, \frac{1}{2})$, $(-\frac{1}{2}, 0, \frac{1}{2})$, $(0, \frac{1}{2}, \frac{1}{2})$, $(0, -\frac{1}{2}, \frac{1}{2})$, $(\frac{1}{2}, 0, -\frac{1}{2})$,

$(-\frac{1}{2}, 0, -\frac{1}{2})$, $(0, \frac{1}{2}, -\frac{1}{2})$, $(0, -\frac{1}{2}, -\frac{1}{2})$, $(\frac{1}{2}, -\frac{1}{2}, 0)$, $(\frac{1}{2}, \frac{1}{2}, 0)$,

$(-\frac{1}{2}, \frac{1}{2}, 0)$ and $(-\frac{1}{2}, -\frac{1}{2}, 0)$,

they contribute altogether three possible occupation sites to the unit cell. The other five sites are at

$(0, 0, 0)$, $(\frac{1}{4}, -\frac{1}{4}, \frac{1}{4})$, $(-\frac{1}{4}, \frac{1}{4}, \frac{1}{4})$, $(\frac{1}{4}, \frac{1}{4}, -\frac{1}{4})$ and $(-\frac{1}{4}, -\frac{1}{4}, -\frac{1}{4})$.

The sixteen octahedral sites of the B sublattice are located at

$(\frac{3}{8}, \frac{1}{8}, \frac{1}{8})$, $(\frac{1}{8}, \frac{3}{8}, \frac{1}{8})$, $(\frac{1}{8}, \frac{1}{8}, \frac{3}{8})$, $(\frac{3}{8}, \frac{3}{8}, \frac{3}{8})$,

$(-\frac{3}{8}, -\frac{1}{8}, \frac{1}{8})$, $(-\frac{1}{8}, -\frac{3}{8}, \frac{1}{8})$, $(-\frac{1}{8}, -\frac{1}{8}, \frac{3}{8})$, $(-\frac{3}{8}, -\frac{3}{8}, \frac{3}{8})$,

$(-\frac{1}{8}, \frac{1}{8}, -\frac{3}{8})$, $(-\frac{1}{8}, \frac{3}{8}, -\frac{1}{8})$, $(\frac{3}{8}, \frac{1}{8}, -\frac{1}{8})$, $(-\frac{3}{8}, \frac{3}{8}, -\frac{3}{8})$,

$(\frac{1}{8}, -\frac{1}{8}, -\frac{3}{8})$, $(\frac{1}{8}, -\frac{3}{8}, -\frac{1}{8})$, $(\frac{3}{8}, -\frac{1}{8}, -\frac{1}{8})$ and $(\frac{3}{8}, -\frac{3}{8}, -\frac{3}{8})$.

The diagram of tetrahedral and octahedral sites in the spinel structure is shown in Fig. 2.8.

Spinel ferrites can be categorized as being normal, inverse or mixed depending on how the divalent and trivalent magnetic ions are arranged among the two types of interstitial sites which form the two sublattices in the spinel structure compounds. Fig. 2.9. is a schematic illustration of the normal and inverse spinel structures. If the divalent ions enter only into the tetrahedrally coordinated sites forming the A sublattice and the trivalent ions enter only into the octahedrally coordinated sites, the spinel is said to be a normal ferrite. An example of a normal spinel compound is $MgAl_2O_4$. When only trivalent ions enter into the A sublattice and equal numbers of the divalent and trivalent ions enter randomly into the B sites, the spinel is in the inverse spinel arrangement. $NiFe_2O_4$ is an example of a ferrite having the inverse arrangement. If, however, both the trivalent and divalent ions enter into both sublattices, the spinel is said to be a mixed spinel. Most mixed spinels result when nonmagnetic ions are substituted for some of the magnetic ions on the B sublattice. Cobalt ferrite, $CoFe_2O_4$, is an example of a mixed ferrite which does not contain any nonmagnetic cations. The degree of mixing or number of divalent Co ions entering into the A sublattice in what would normally be an inverse arrangement depends on the prior heat treatment of the $CoFe_2O_4$ crystal. Sawatzky, et al.(1969),

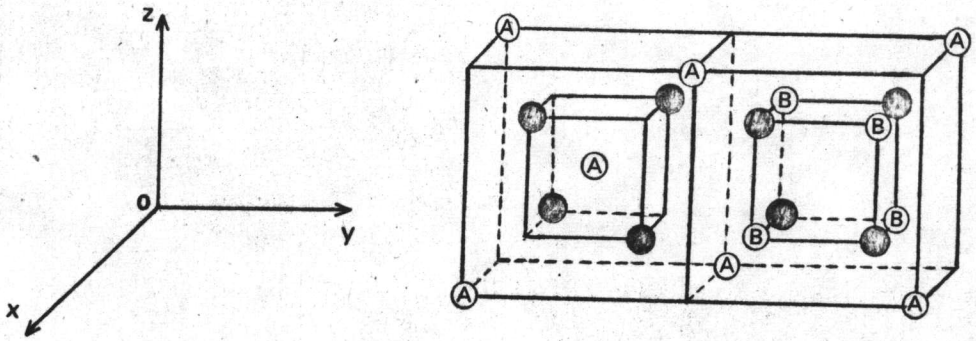

Fig 2.8. A spinel structure. The circles with A represent tetrahedral sites, the circles with B are for octahedral and the black circles indicate oxygen ions. Only two octants of a unit cell is shown. The other octants have either of these structures and are arranged so that no two adjacent octants have the same configuration.

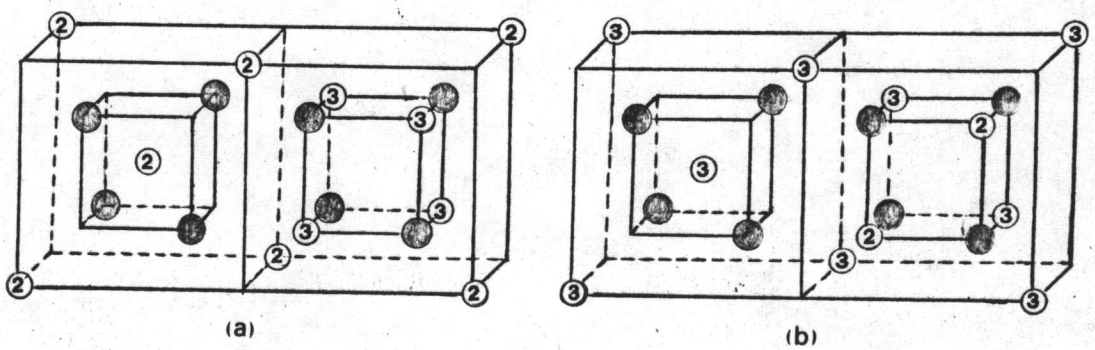

Fig. 2.9. Spinel structures. (a) Normal spinel structure and (b) inverse spinel structure. A circle with the number 2 indicates a divalent ion and the one with the number 3 indicates a trivalent ion while a solid dot stands for an oxygen ion.

have indicated that the temperature at which the crystal was being formed is related to concentration of Co^{2+} ions on the A sublattice and the relationship is approximated by

$$x\,(1 + x)/(1 - x)^2 \;\alpha\; e^{\frac{1}{T}} \qquad (2.3.1).$$

If x is the concentration of Co^{2+} ions on the A sublattice, then the cation arrangement is $(Co_x^{2+}\ Fe_{1-x}^{3+})\left[Co_{1-x}^{2+}\ Fe_{1+x}^{3+}\right]O_4$, where ( ) denotes the A sites and [ ] denotes the B sites.

Tang (1977) has proposed an extension of a molecular field method introduced by Kaneyoshi (1970) for studying the hyperfine fields in the mixed ferrimagnetic compound $CoFe_2O_4$. The molecular field occurs resulting from the superexchange interactions between the magnetic ions at the sites of the crystal. The interactions between the magnetics ions situated on the nearest neighbor A and B sites should be larger than interactions between ions on the nearest neighbor A-A sites and between ions on the nearest neighbor B-B sites since the angle of A-anion-B is favourable for the superexchange mechanism while the angles of A-anion-A and B-anion-B are not. In addition, the next-nearest-neighbor covalent-spin-transfer interaction for the Co^{2+} ions on next nearest neighbor B-B sites should be taken into account. For the $CoFe_2O_4$ spinel ferrites, this means that there are five exchange integrals (or coupling constants):

$J_{ij}^{(1)}\,(Co_i^{2+}, Co_j^{2+})$, $J_{ij}^{(2)}\,(Co_i^{2+}, F_j^{3+})$, $J_{ij}^{(3)}(Fe_i^{3+}, Co_j^{2+})$, $J_{ij}^{(4)}(Fe_i^{3+}, Fe_j^{3+})$, and $J_{jj'}^{(5)}\,(Co_j^{2+}, Co_{j'}^{2+})$ (the subscript i(j) denotes the fact that the

ion is on the A(B) sublattice and ' denotes the nearest neighbor lattice). To account for the observed spin arrangement, the four inter-lattice superexchange interactions must be antiferromagnetic in nature, while the intralattice interaction $J^{(5)}_{jj'}$ is ferromagnetic. Therefore, if we assume the spin Hamiltonian of $CoFe_2O_4$ is Heisenberg-like, the Hamiltonian becomes

$$\mathcal{H} = -2\sum_{i,j} J^{(1)}_{ij} \vec{A}_i \cdot \vec{C}_j a_i c_j - 2\sum_{i,j} J^{(2)}_{ij} \vec{A}_i \cdot \vec{D}_j a_i d_j$$

$$- 2\sum_{i,j} J^{(3)}_{ij} \vec{B}_i \cdot \vec{C}_j b_i c_j - 2\sum_{i,j} J^{(4)}_{ij} \vec{B}_i \cdot \vec{D}_j b_i d_j$$

$$- 2\sum_{j,j'} J^{(5)}_{jj'} \vec{C}_j \cdot \vec{C}_{j'} c_j c_{j'} \qquad (2.3.2).$$

In eq. (2.3.2), $\vec{A}_i$ is the spin operator for a Co^{2+} ion located on the i-th site in A sublattice;

$\vec{B}_i$ is the spin operator for a Fe^{3+} ion located on the i-th site in A sublattice;

$\vec{C}_j$ is the spin operator for a Co^{2+} ion located on the j-th site in B sublattice;

$\vec{D}_j$ is the spin operator for a Fe^{3+} ion located on the j-th site in B sublattice,

and a_i, b_i are the site occupancy operators for a Co^{2+}, Fe^{3+} ion on the i-th site of the A sublattice, and c_j, d_j are the site occupancy operators for a Co^{2+}, Fe^{3+} ion on the j-th site of the B sublattice respectively. Remember that

$a_i = 1$ if the i-th site is occupied by a Co^{2+} ion,

$= 0$ if the i-th site is not occupied by a Co^{2+} ion,

$b_i = 1$ if the i-th site is occupied by a Fe^{3+} ion,

$= 0$ if the i-th site is not,

etc,

and that all the sites must be occupied by either a Co^{2+} ion or a Fe^{3+} ion, the site occupancy operators a_i and b_i are related to each other. The two relationships are

$$a_i = 1 - b_i ,$$

$$c_j = 1 - d_j \qquad (2.3.3).$$

The configuration averages (denoted by a subscript r) of these sites are in turn related to x, the concentration of Co^{2+} ion on the A sublattice, i.e.,

$$\langle a_i \rangle_r = a = x$$

$$\langle b_i \rangle_r = b = 1 - x$$

$$\langle c_j \rangle_r = c = \frac{1 - x}{2}$$

$$\langle d_j \rangle_r = d = \frac{1 + x}{2} \qquad (2.3.4).$$

To obtain the effective fields acting on an individual spin located on any site k, we introduce the mean field approximation

$$2 \sum_{i,j} J_{ij} \vec{A}_i \cdot \vec{B}_j = \sum_{i,j} J_{ij} \vec{A}_i \cdot \langle \vec{B}_j \rangle + \sum_{i,j} J_{ij} \vec{B}_j \cdot \langle \vec{A}_i \rangle \qquad (2.3.5),$$

where $\langle \quad \rangle$ denotes an ensemble average. With this approximation,

the effective magnetic fields acting on the Co_i^{2+}, Fe_i^{3+}, Fe_j^{3+} and Co_j^{2+} spins are

$$H_{eff}(\vec{A}_i) = \sum_j J_{ij}^{(1)} \langle \vec{C}_j \rangle c_j + \sum_j J_{ij}^{(2)} \langle \vec{D}_j \rangle d_j \qquad (2.3.6a),$$

$$H_{eff}(\vec{B}_i) = \sum_j J_{ij}^{(3)} \langle \vec{C}_j \rangle c_j + \sum_j J_{ij}^{(4)} \langle \vec{D}_j \rangle d_j \qquad (2.3.6b),$$

$$H_{eff}(\vec{D}_j) = \sum_i J_{ij}^{(2)} \langle \vec{A}_i \rangle a_i + \sum_i J_{ij}^{(4)} \langle \vec{B}_i \rangle b_i \qquad (2.3.6c),$$

and

$$H_{eff}(\vec{C}_j) = \sum_i J_{ij}^{(1)} \langle \vec{A}_i \rangle a_i + \sum_i J_{ij}^{(3)} \langle \vec{B}_i \rangle b_i + \sum_{j'} J_{jj'}^{(5)} \langle \vec{C}_{j'} \rangle c_{j'} \qquad (2.3.6d).$$

It should be understood that the above effective fields are for a $CoFe_2O_4$ ferrite having a definite arrangement of Co^{2+} and Fe^{3+} ions on the A and B sublattice. Since any arrangement of the Co^{2+} and Fe^{3+} ions is possible as long as the concentration of the Co^{2+} ions on the A sublattice is x, the effective fields must be averaged over all possible arrangements, i.e., a configuration average must be taken.

The configuration averages can be calculated by using a trick introduced by Kaneyoshi (1970). He used the fact that in the Neel-Weiss molecular field approximation, the ensemble average of a spin $\vec{S}_k$,

$$\langle \vec{S}_k \rangle = S B_S(S \beta H_{eff}(\vec{S}_k)) \qquad (2.3.7a)$$

can be rewritten as

$$\langle \vec{S}_k \rangle = S \int_{-\infty}^{\infty} B_S(S\beta E)\, \delta(E - H_{eff}(\vec{S}_k))\, dE \qquad (2.3.7b),$$

where $B_S(X)$ is the Brillouin function ; S, the spin quantum number; $H_{eff}(\vec{S}_k)$, the effective field acting on a spin $\vec{S}_k$ located on the k-th site; $\delta(X)$, the Dirac delta function and $\beta = (k_B T)^{-1}$. Here, He introduces the auxiliary function defined by

$$G_k(E) = \left[E - H_{eff}(\vec{S}_k) \right]^{-1} \qquad (2.3.8a),$$

which is related to a δ - function through

$$\delta(E - H_{eff}(\vec{S}_k)) = \lim_{\varepsilon \to +0} \frac{i}{2\pi} \left[G_k(E + i\varepsilon) - G_k(E - i\varepsilon) \right] \qquad (2.3.8b).$$

Eq. (2.3.7b) can be rewritten as

$$\langle \vec{S}_k \rangle = S \int_{-\infty}^{\infty} B_S(S\beta E) \left\{ \lim_{\varepsilon \to 0^+} \frac{i}{2\pi} \left[G_k(E + i\varepsilon) - G_k(E - i\varepsilon) \right] \right\} dE \qquad (2.3.9).$$

Thus the configuration average of $\langle \vec{S}_k \rangle$ reduces to finding the configuration averages of the auxiliary function $G_k(E \pm i\varepsilon)$.

After performing the configuration averages, we get

$$\langle\langle \vec{A} \rangle\rangle_r = \frac{1}{2} A \left\{ B_A(A\beta E_+) + B_A(A\beta E_-) \right\} \qquad (2.3.10a),$$

$$\langle\langle \vec{B} \rangle\rangle_r = \frac{1}{2} B \left\{ B_B(B\beta E'_+) + B_B(B\beta E'_-) \right\} \qquad (2.3.10b),$$

$$\langle\langle \vec{D} \rangle\rangle_r = \frac{1}{2} D \left\{ B_D(D\beta E''_+) + B_D(D\beta E''_-) \right\} \qquad (2.3.10c),$$

$$\langle\langle \vec{C} \rangle\rangle_r = \frac{1}{2} C \left\{ B_C(C\beta E'''_+) + B_C(C\beta E'''_-) \right\} \qquad (2.3.10d),$$

where A, C and B, D are the spin quantum number of Co^{2+} and Fe^{3+} ions on the sites in the two sublattices, respectively, and where

$$E\pm = Z_2 J^{(1)}(0) \ll \vec{C} \gg_r P_1(c) + Z_2 J^{(2)}(0) \ll \vec{D} \gg_r P_1(d)$$

$$\pm\sqrt{P_2(d)\ \frac{1}{N_B}\ \sum_K \left| J^{(2)}(K) \ll \vec{D} \gg_r - J^{(1)}(K) \ll \vec{C} \gg_r \right|^2} \qquad (2.3.11a),$$

$$E\pm' = Z_2 J^{(3)}(0) \ll \vec{C} \gg_r P_1(c) + Z_2 J^{(4)}(0) \ll \vec{D} \gg_r P_1(d)$$

$$\pm\sqrt{P_2(d)\ \frac{1}{N_B}\ \sum_K \left| J^{(4)}(K) \ll \vec{D} \gg_r - J^{(3)}(K) \ll \vec{C} \gg_r \right|^2} \qquad (2.3.11b),$$

$$E\pm'' = Z_1 J^{(2)}(0) \ll \vec{A} \gg_r P_1(a) + Z_1 J^{(4)}(0) \ll \vec{B} \gg_r P_1(b)$$

$$\pm\sqrt{P_2(b)\ \frac{1}{N_A}\ \sum_K \left| J^{(4)}(K) \ll \vec{B} \gg_r - J^{(2)}(K) \ll \vec{A} \gg_r \right|^2} \qquad (2.3.11c),$$

$$E\pm''' = Z_1 J^{(1)}(0) \ll \vec{A} \gg_r P_1(a) + Z_1 J^{(3)}(0) \ll \vec{B} \gg_r P_1(b) + Z_3 J^{(5)}(0) P_1(c)$$

$$\pm\sqrt{P_2(b)\ \frac{1}{N_A}\ \sum_K \left| J^{(3)}(K) \ll \vec{B} \gg_r - J^{(1)}(K) \ll \vec{A} \gg_r \right|^2 + P_2(c) \frac{1}{N_B} \left(\ll \vec{C} \gg_r \right)^2 \sum_K \left| J^{(5)}(K) \right|^2}$$

(2.3.11d).

In the eqs. (2.3.11a) - (2.3.11d), Z_1 (Z_2) is the number of A(B) sites on the nearest neighbor shell of a B(A) site, N_A (N_B) is the number of sites in A(B) sublattice (note also that $N_B = 2N_A$), and $P_1(a) = a$, $P_1(b) = b$,

$P_1(c) = c$, and $P_1(d) = d$ which are related to x by the eq. (2.3.4) and $P_2(a) = (a - a^2)$, ... , $P_2(d) = (d - d^2)$, respectively.

Eqs. (2.3.10a) - (2.3.10d) form a set of simultaneous nonlinear algebraic equations. The behaviour of the configuration averages spins as the temperature is changed can be determined by numerical methods.

The effective local magnetic fields acting on any given site in the A and B sublattice, would be the configuration average of eqs. (2.3.6a) - (2.3.6d). All of the quantities in these equations are replaced by their configuration averages. This means that

$$\langle H_{eff}(\vec{A}_i)\rangle_r = N_B J^{(1)} \langle\langle \vec{C} \rangle\rangle_r \frac{(1-x)}{2} + N_B J^{(2)} \langle\langle \vec{D} \rangle\rangle_r \frac{(1+x)}{2} \quad (2.3.12a),$$

$$\langle H_{eff}(\vec{B}_i)\rangle_r = N_B J^{(3)} \langle\langle \vec{C} \rangle\rangle_r \frac{(1-x)}{2} + N_B J^{(4)} \langle\langle \vec{D} \rangle\rangle_r \frac{(1+x)}{2} \quad (2.3.12b),$$

$$\langle H_{eff}(\vec{D}_j)\rangle_r = N_A J^{(2)} \langle\langle \vec{A} \rangle\rangle_r x + N_A J^{(4)} \langle\langle \vec{B} \rangle\rangle_r (1-x) \quad (2.3.12c),$$

$$\langle H_{eff}(\vec{C}_j)\rangle_r = N_A J^{(1)} \langle\langle \vec{A} \rangle\rangle_r x + N_A J^{(3)} \langle\langle \vec{B} \rangle\rangle_r (1-x) - N_B J^{(5)} \langle\langle \vec{C} \rangle\rangle_r \frac{(1-x)}{2} \quad (2.3.12d),$$

where values of $\langle a_i \rangle_r$, $\langle b_i \rangle_r$, $\langle c_j \rangle_r$ and $\langle d_j \rangle_r$ have been expressed in term of the concentration, x, of cobalt ions on the A sublattice.

We can rewrite the effective local magnetic fields acting on the Fe^{3+} ions from eqs. (2.3.12b) and (2.3.12c) as

$$\langle H_{eff}(Fe^{3+}A)\rangle_r = \frac{1}{2} N_B \left[J^{(3)} \ll Co_B^{2+} \gg_r + J^{(4)} \ll Fe_B^{3+} \gg_r \right]$$

$$- \frac{x}{2} N_B \left[J^{(3)} \ll Co_B^{2+} \gg_r - J^{(4)} \ll Fe_B^{3+} \gg_r \right] \quad (2.3.13a),$$

$$\langle H_{eff}(Fe_B^{3+})\rangle_r = N_A J^{(4)} \ll Fe_A^{3+} \gg_r - x N_A \left[J^{(4)} \ll Fe_A^{3+} \gg_r \right.$$

$$\left. - J^{(2)} \ll Co_A^{2+} \gg_r \right] \quad (2.3.13b).$$

However, the dependence of $\langle H_{eff} (Fe_A^{3+}) \rangle_r$ and $\langle H_{eff} (Fe_B^{3+}) \rangle_r$ on the concentration x are not immediately evident since $\ll Fe_A^{3+} \gg_r$, $\ll Fe_B^{3+} \gg_r$, $\ll Co_A^{2+} \gg_r$ and $\ll Co_B^{2+} \gg_r$ are also dependent on x. Significance of eqs. (2.3.13a) and (2.3.13b) in light of some experimental data taken by Sawatzky, it al. (1969) will be given in Chapter VI.